Polyelectrolyte Complexes Stabilize and Controllably Release Vascular Endothelial Growth Factor

Min Huang,[†] Samadhi N. Vitharana,[‡] Laura J. Peek,[†] Tina Coop,[‡] and Cory Berkland*[,†,‡]

Department of Pharmaceutical Chemistry and Department of Chemical and Petroleum Engineering, The University of Kansas, Lawrence, Kansas 66047

Received December 21, 2006; Revised Manuscript Received February 20, 2007

Angiogenesis has long been a desired therapeutic approach to improve clinical outcomes of conditions typified by ischemia. Vascular endothelial growth factor (VEGF) has demonstrated the ability to generate new blood vessels in vivo, but trials using intravenous delivery have not yet produced clinical success. Localized, sustained delivery of VEGF has been proven necessary to generate blood vessels as demonstrated by implantable, controlled release devices. Ultimately, nanoparticles delivered by intravenous injection may be designed to accumulate in target tissues and sustain the local VEGF concentration; however, injectable nanosuspensions that control the release of stabilized VEGF must first be developed. In this study, we utilize the heparin binding domain of VEGF to bind the polyanion dextran sulfate, resulting in an enhanced thermal stability of VEGF. Coacervation of the VEGF-bound dextran sulfate with selected polycations (chitosan, polyethylenimine, or poly-L-lysine) produced nanoparticles ~250 nm in diameter with high VEGF encapsulation efficiency (50−85%). Release of VEGF from these formulations persisted for >10 days and maintained high VEGF activity as determined by ELISA and a mitogenic bioassay. Chitosan−dextran sulfate complexes were preferred because of their biodegradability, desirable particle size (~250 nm), entrapment efficiency (~85%), controlled release (near linear for 10 days), and mitogenic activity.

Introduction

Over the past 30 years, arterio- and angiogenesis have been vaunted as a therapeutic approach to reduce the pathological consequence of myocardial ischemia, wounds, neuropathy, retinopathy, transplant failure, etc.[1−3] Despite the complexity of angiogenic signaling pathways, vascular endothelial growth factor (VEGF) has emerged as a potent angiogenic cytokine. Unfortunately, clinical trials investigating intravenous (IV) administration of VEGF have not yet demonstrated sufficient efficacy above placebo control groups to garner FDA approval.[4] Most researchers have suggested that the spatial and temporal resolution of VEGF administration must be controlled to target development of mature blood vessels.[5,6]

Although VEGF has repeatedly been shown to generate new blood vessels in vivo,[4] several problems exist in the IV administration of this powerful neovascular agent. Because sustained local concentrations are required to develop mature blood vessels, the short circulation half-life, extraneous interactions with multiple binding sites (e.g., VEGF receptors, heparin, etc.), and ultimate degradation of VEGF are problematic.[7−10] In addition, systemic IV administration of the growth factor may result in nonspecific angiogenesis, potentially propagating conditions such as hypotension, edema, etc.[11−13] These facts have thus far precluded IV injection or infusion as a viable means to deliver VEGF. For example, the VIVA study represented the first randomized, double-blind, placebo-controlled clinical trial using IV delivery of recombinant human VEGF for therapeutic angiogenesis.[14] No statistically significant difference in patient performance was seen above placebo levels, although each study group demonstrated some functional improvement.

Controlled release strategies have demonstrated the importance of maintaining precise concentrations of active growth factors over days or weeks and orchestrating the timing of growth factor release proximal to the site of desired angiogenesis.[15,16] Reports have shown that growth factors like VEGF can promote localized angiogenesis in vivo if administered in a microparticle depot, engineered polymer matrix, or viral vector genetically encoding for VEGF.[7,15,17−19] Each of these methods has the potential to localize VEGF and to deliver VEGF at a more constant rate, leading to site-specific angiogenesis. IV injections or infusions of VEGF are not capable of this kind of precise delivery of growth factors over extended periods of time; however, IV injection may be preferred by physicians as compared to more rigorous device implantation.

Nanoparticles may provide a promising mechanism for targeted angiogenesis via IV administration. Currently, research efforts are extending nanoparticle circulation half-life, avoiding immunological responses commonly associated with particulate vectors, and accurately targeting nanoparticles in vivo.[20−23] By using antibodies or RGD peptides, nanoparticles carrying therapeutic small molecules, proteins, or nucleotides have been targeted to integrins and VEGF receptors to locally deliver payloads of angiogenic or anti-angiogenic factors.[21,23−25] In addition, nanoparticles utilizing biodegradable materials offer the potential to sustain the release of growth factors over a period of days to weeks.[7,26] Current techniques often produce nanoparticles by employing harsh organic solvents, synthetic polymers, or surfactants having high toxicity or immunological activity.[27] Many nanoparticle-forming materials, such as poly(DL-lactic-*co*-glycolic acid), often exhibit low protein loading, routinely demonstrate poor encapsulation efficiency and rapid

* To whom correspondence should be addressed. Phone: (785) 864-1455. Fax: (785) 864-1454. E-mail: berkland@ku.edu.
[†] Department of Pharmaceutical Chemistry.
[‡] Department of Chemical and Petroleum Engineering.

10.1021/bm061211k CCC: $37.00
Published on Web 04/12/2007

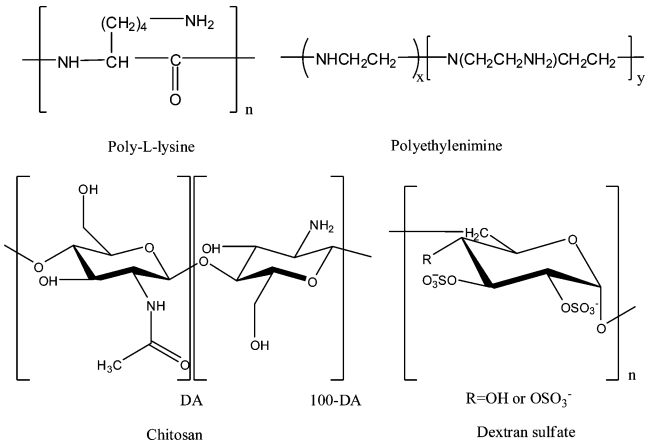

Figure 1. Structures of poly-L-lysine, polyethylenimine, chitosan, and dextran sulfate.

initial release of protein, and may require special formulation to maintain protein stability.[7,28]

We report a method for efficiently encapsulating and stabilizing VEGF using complex coacervation of dextran sulfate and selected polycations (chitosan, polyethylenimine, and poly-L-lysine) to form polyelectrolyte complexes. This work builds upon previous work utilizing polyelectrolyte complexes for drug delivery by Middaugh et al.[29−32] VEGF possesses a heparin binding domain with a high affinity for polyanions.[7,33,34] The polyanion, dextran sulfate, bound VEGF thereby promoting effective nanoparticle loading, acceptable encapsulation efficiency, and enhanced VEGF thermal stability. Of the polyelectrolyte complexes studied, dextran sulfate and chitosan were especially attractive because these materials are biodegradable, offer low toxicity,[35,36] and can be self-assembled to yield particles ~250 nm suitable for IV administration.[37] Specifically, dextran sulfate/chitosan nanoparticles possessed the highest VEGF encapsulation efficiency (~85%) and released native VEGF for >10 days. Ultimately, this formulation serves to protect VEGF for sustained delivery as a platform for future efforts toward targeting these nanocarriers.

Materials and Methods

Materials. Recombinant human VEGF isoform 165 was graciously supplied by Genentech, Inc. Chitosan (M_w = 15 kDa, 84% deacetylated, Polysciences, Inc.), dextran sulfate (M_w = 500 kDa, Fisher Scientific), polyethylenimine (M_w = 10 kDa, Aldrich), and poly-L-lysine (M_w = 10 kDa, Sigma) (Figure 1) were used as obtained without further purification. Zinc sulfate heptahydrate (Sigma) was used as a nanoparticle cross-linker in some experiments. Microsep centrifugal devices (Pall Life Sciences), dialysis membranes (Spectrum), side-A-lyzer dialysis cassettes (Pierce), and mannitol (Sigma) were used during particle purification.

Preparation of Polyelectrolyte Complex Nanoparticles. A sample of VEGF was diluted (1:3, v/v) in 50 mM phosphate buffer, pH 7.0, and dialyzed into the same buffer using a dialysis cassette with a 10 000 MWCO (Pierce) overnight. The concentration of the recovered sample (~1 mg/mL) was determined by UV spectroscopy. To prepare VEGF-loaded polyelectrolyte complex (PEC) nanoparticles, 80 μL of the recovered sample was added to 800 μL of 1% (w/v) dextran sulfate solution (in water) and stirred at 600 rpm for 30 min. Next, 1.6 mL of the appropriate polycationic solution (0.1% w/v) was added dropwise and stirred for another 5 min. Chitosan was dissolved in acetic buffer (pH ≈ 6) and added dropwise to the dextran sulfate solution. Finally, 80 μL of zinc sulfate solution (1 M) was added and stirred for 30 min.[32] The prepared particles were dialyzed into 50 mM phosphate buffer with 5% mannitol, for 24 h in the dark. The dialyzed sample was filtered through a 0.8 μm filter and lyophilized to obtain a dry powder.

Characterization of Polyelectrolyte Nanoparticles. The mean particle size was determined by dynamic light scattering experiments employing a ZetaPALS Zeta Potential Analyzer (Brookhaven Instruments Corp.). An aliquot of lyophilized particles was suspended in water, and three consecutive 1 min measurements were obtained by detecting light scattering at a 90° angle. The mean effective diameter and polydispersity were determined by the method of cumulants.[38] The surface charge (zeta potential) of the particles was investigated by phase analysis light scattering using the same instrument. Samples were prepared by dispersing 5 mg of the lyophilized nanoparticles in 1 mL of deionized water (Barnstead Nanopure). Three measurements were taken for each sample.

The morphology of the particles was examined by transmission electron microscopy (JEM-1200EXII, JEOL). The lyophilized particles were dialyzed into deionized water for 24 h using dialysis tubing (SpectroPro MWCO 15 000; Spectrum Laboratories, CA) to remove mannitol from the sample. Seven microliters of the dialyzed sample and 3 μL of 2% (w/v) phosphotungstate solution were placed on a 300 mesh copper grid with a carbon-coated Formvar membrane. The sample was allowed to sit for ~2 min, and the excess water was removed with No. 1 Whatman filter paper. The sample was kept in a desiccator overnight and examined by TEM.

Biophysical Characterization of VEGF, VEGF Bound to DS, and VEGF in PEC Nanoparticles. *Differential Scanning Calorimetry*. Calorimetric experiments were performed with a MicroCal VP-DSC high throughput capillary differential scanning calorimeter (Northampton, MA). DSC thermograms were obtained from 10 to 115 °C at a scan rate of 1 °C/min with VEGF, VEGF bound to DS, VEGF PEC nanoparticles, and unloaded PEC nanoparticles. Baseline correction was performed by subtracting a buffer thermogram obtained under identical conditions. The data were analyzed using Microcal Origin 7.0 (OriginLab Corp., Northampton, MA).

Circular Dichroism. Far-UV spectra were collected using a Jasco 810 spectropolarimeter equipped with a Peltier temperature controller (Jasco, Easton, MD). Protein samples (0.1 mg/mL) were analyzed at 37 °C in a quartz cuvette with a 0.1 cm path-length. Spectra were collected at a scan rate of 10 nm/min and a resolution of 0.5 nm using a response time of 2 s and a bandwidth of 1 nm. To monitor changes in the secondary structure of VEGF bound with DS or in nanoparticles, CD spectra were obtained for VEGF in the presence of a 10-fold or 50-fold weight excess of dextran sulfate or loaded in PEC nanoparticles. Spectra for VEGF bound with DS were background corrected with respect to DS in buffer, and spectra for VEGF-loaded nanoparticles were background corrected with respect to unloaded nanoparticles. The thermal unfolding of the proteins was followed by monitoring the CD signal at 208 nm over a temperature range of 10−90 °C with a resolution of 0.5 and a 15 °C/h heating rate. The protein concentration was 0.1 mg/mL for all measurements. CD signal was converted to molar ellipticity, and the thermal transitions were analyzed using the Jasco Spectra Manager and MicroCal Origin v.7.0 software.

Fourier Transform Infrared Spectroscopy. The physical structures of VEGF, VEGF−DS, VEGF PECs, and all individual components of the complexes were evaluated using Fourier transform infrared (FTIR) spectroscopy. Samples of each component contained 1% (w/v) dextran sulfate, 5 mg/mL VEGF, 2% (w/v) chitosan, and 1% (w/v) PEI or poly-L-lysine. The PEC nanoparticle samples contained less than 0.03 mg/mL VEGF, 0.3% dextran sulfate (DS), and 0.06% chitosan, PEI, or poly-L-lysine. Samples were run using attenuated total reflectance employing a 45° ZnSe trough plate with volatile liquid cover. Data were collected using a Bomem PROTA FTIR protein analyzer (Norwalk, CT) to acquire spectra using 256 scans from 700 to 4000 cm^{-1} with a resolution of 4 cm^{-1}. VEGF and VEGF−DS samples contained buffer, while all other samples were run in distilled−deionized water. A spectrum of water or buffer was subtracted from each sample

spectrum by eliminating the association band of water at 2200 cm^{-1} using Omnic software.

High-Resolution Derivative UV Absorbance Spectroscopy. UV absorbance temperature perturbation studies were conducted with an Agilent (Palo Alto, CA) 8453 diode array UV−visible spectrophotometer. Spectra were collected using an integration time of 25 s over a range of 10 to 90 °C at 2.5 °C intervals. A 5 min equilibration was included before collection of each spectrum to allow for sufficient time to equilibrate temperature. Spectral analysis was conducted using Chemstation software (Agilent). Second derivative spectra were conducted using a nine-point data filter and fifth degree Savitzky-Golay polynomial, and subsequently fitted to a cubic function, with 99 interpolated points per raw data point, permitting 0.01 nm resolution. Peak positions were determined from the interpolated curves using Microcal Origin7.0. A 1 cm path length capped cuvette was used with a total sample of 200 μL of protein sample at 0.2 mg/mL. The spectrum of VEGF−DS was also conducted in the same manner except that the DS solution was used as a blank to remove interference from DS.

VEGF Loading, Entrapment Efficiency, and Release from PEC Nanoparticles. VEGF loading into polyelectrolyte nanoparticles was calculated by an indirect method where VEGF concentration was determined in purified supernatant and subtracted from the initial amount entered into the experiment. Several methods were attempted to directly measure VEGF encapsulation by disrupting nanoparticles with sodium dodecyl sulfate, high sodium chloride concentration, and low pH; however, no method proved as accurate as the indirect method. After particles were made, they were centrifuged at 15 000*g* for 45 min, and the supernatant was separated for analysis. The amount of VEGF in the original VEGF sample used to make particles and the supernatant was determined by UV spectroscopy (Agilent 8453) based on an extinction coefficient of 0.37 mg^{-1} mL cm^{-1} for VEGF at 276 nm. To determine the VEGF release kinetics, ~10 mg of lyophilized sample was resuspended in 50 mM phosphate buffer (pH 7.0) within Microsep centrifugal devices (MWCO = 100 000 Da) and incubated at 37 °C while being shaken at 150 rpm. The vial was centrifuged at 4000*g* for 1 h, and the solution containing the released protein was collected and analyzed by BCA assay. Active VEGF content in the released protein was determined by an enzyme-linked immunosorbent assay (ELISA) and measured in triplicate. The ELISA measured the concentration of "active" VEGF, that is, VEGF maintaining binding affinity to the polyclonal antibody. Plates precoated with polyclonal antibody were used to capture VEGF in each sample. After washing, biotinylated monoclonal antibody specific for VEGF was added, which bound to the immobilized VEGF captured during the first incubation. Biotinylated VEGF specifically bound with a streptavidin-peroxidase enzyme, which allowed for chromogenic detection at 450 nm upon addition of substrate, tetramethylbenzidine. The assay has a detection range between 5 pg/mL and 3 ng/mL. The optical density of the samples was read at 450 nm with a microplate reader (Spectramax M5, Molecular Device). Eight standard VEGF solutions were used to prepare the standard curve. VEGF released from PEC nanoparticles was determined by ELISA and BCA, respectively. The percentage of "active" protein was determined by dividing the VEGF concentration determined by ELISA by the VEGF concentration determined by BCA.

Mitogenic Bioassay of VEGF and PEC Nanoparticles Entrapping VEGF. The activity of VEGF either in solution or released from nanoparticles was determined using a cell proliferation assay. Briefly, human umbilical cord vascular endothelial cells (HUVEC) were seeded in 96-well tissue culture plates in DMEM medium supplemented with 2% heat inactivated bovine serum at a density of 2000 cells/well. Cells were incubated with 100 ng/mL of VEGF either in solution or in nanoparticles. A Cell Titer 96 aqueous cell proliferation assay kit (Promega, Madison, WI) was used to quantify the viable cells. The cell proliferation was determined at different time points over a period of 5 days posttreatment. At ~5 days, cells began to form a continuous monolayer, and contact inhibition of cell proliferation confounded further analysis. To determine VEGF concentration in the medium of cells treated either with VEGF solution or with VEGF nanoparticles, the medium from each well was collected, centrifuged at 13 000 rpm for 10 min, and the supernatant was analyzed for VEGF using the ELISA described before. Statistical significance was calculated using one-way analysis of variance (ANOVA) with Tukey's comparison post test.

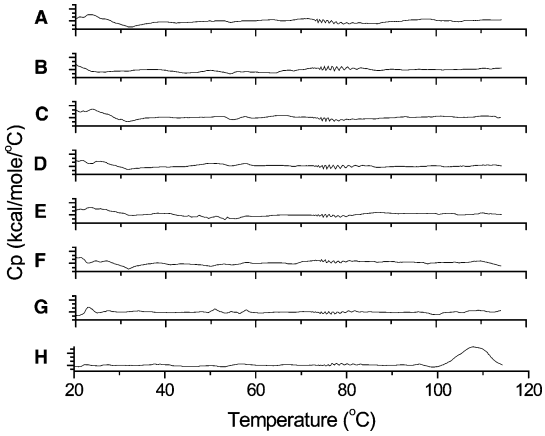

Figure 2. Differential scanning calorimetry thermograms of (A) loaded PLL−DS, (B) unloaded PLL−DS, (C) loaded PEI−DS, (D) unloaded PEI−DS, (E) loaded CS−DS, (F) unloaded CS−DS, (G) VEGF bound to DS, and (H) VEGF. "Loaded" denotes VEGF inclusion into the formulations according to the reported methods.

Results

Stabilization of VEGF by Binding Dextran Sulfate. VEGF thermal stability may be improved in formulations through the addition of polyanions, which associate with the heparin binding domain of VEGF.[33,34] Differential scanning calorimetry thermograms indicated a shift in the melting temperature of VEGF when mixed with 1% w/v dextran sulfate (Figure 2). VEGF by itself showed very high thermal stability with a melting temperature (T_m) of about 107 °C (Figure 2H). This unusually high thermal stability is largely due to the unique cystine knot motif that essentially cross-links the protein tertiary structure.[39] VEGF bound to dextran sulfate did not show any transition, suggesting that the thermal stability of VEGF was increased above the range of our instrument (115 °C) upon binding to dextran sulfate (Figure 2G). Dextran sulfate alone did not possess a thermal transition of any kind for the conditions studied (data not shown). Similarly, VEGF-loaded and unloaded nanoparticles did not show any thermal transition peak within this temperature range (Figure 2A−F).

Far-UV CD was employed to explore the secondary structure of VEGF in the presence and absence of dextran sulfate and within nanoparticles. The unbound form of VEGF possessed a negative peak around 208 nm (Figure 3A). Based on the fact that β-sheet and type-I β-turn structures give rise to negative peaks at 215 and 205 nm, respectively, the negative peak at 208 nm for VEGF suggests a mixture of β-sheet and β-turn structures within the protein as has been confirmed in the crystal structure.[40] The secondary structure was quantified by deconvolution of the CD spectrum using the program CTSSTR provided by Dichroweb software and revealed a high percentage of β-sheet structure (33%) and β-turn structure (25%). VEGF bound to dextran sulfate (β-sheet, 39%; β-turn, 23%) and inside the PEC nanoparticles revealed similar CD spectra, which overlapped quite well with the unbound form of VEGF, suggesting negligible perturbation of the secondary structure of VEGF upon binding to dextran sulfate and formulating into

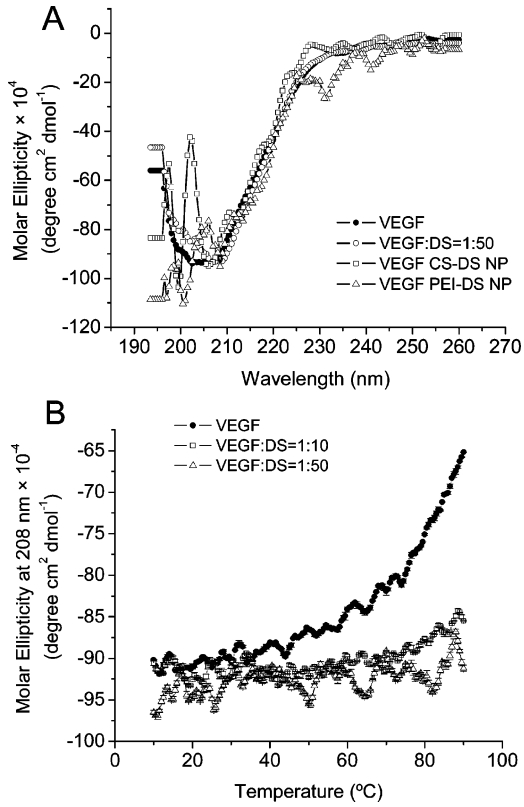

Figure 3. (A) CD spectra of VEGF, VEGF bound with DS, and VEGF entrapped in PEC nanoparticles. (B) The effect of temperature on the molar ellipticity of VEGF as monitored at 208 nm by CD ($n = 2$).

nanoparticles.[41,42] Although the CD spectrum for VEGF in the PEC nanoparticles showed relatively large fluctuations below 210 nm, potentially due to interference of the polymer and/or the relative opacity of the nanoparticle suspension, the negative peak around 208 nm remains visible, suggesting significant β-sheet content was retained (Figure 3A).

Temperature-induced changes in the secondary structure of VEGF were also evaluated by monitoring changes in CD signal at 208 nm (Figure 3B). For VEGF, an increase in molar ellipticity was observed as the temperature was increased, suggesting a loss of VEGF secondary structure. In contrast, VEGF bound to DS showed unchanged secondary structure over the temperature range evaluated, indicating that DS effectively stabilizes VEGF.

The second-derivative UV absorbance spectrum of VEGF exhibited three distinct negative peaks, all of which were monitored as a function of temperature. At 10 °C, the negative peaks occurred approximately at 258 nm (Phe), 268 nm (Phe/Tyr), and 276 nm (Tyr). Changes in the microenvironment of these residues induced changes in their spectral characteristics, thus providing a tool for analyzing the tertiary structural stability. Peaks associated with Tyr/Trp and Trp were not evident in the second-derivative UV absorbance spectrum because VEGF does not possess any Trp amino acids. With the increase of temperature, the peak positions for these amino acids all shifted to longer wavelengths (Figure 4). The Phe peak showed the most significant shift (~1.5 nm) and provided the most distinctive assay of the tertiary structure of VEGF (Figure 4A). For all three amino acid peaks, VEGF bound with DS generally showed a decreased red shift, especially for the Phe peak at 258 nm, which remained almost unchanged over the temperature range studied. These results indicated that the tertiary structure of VEGF was thermally stabilized through binding to dextran sulfate.

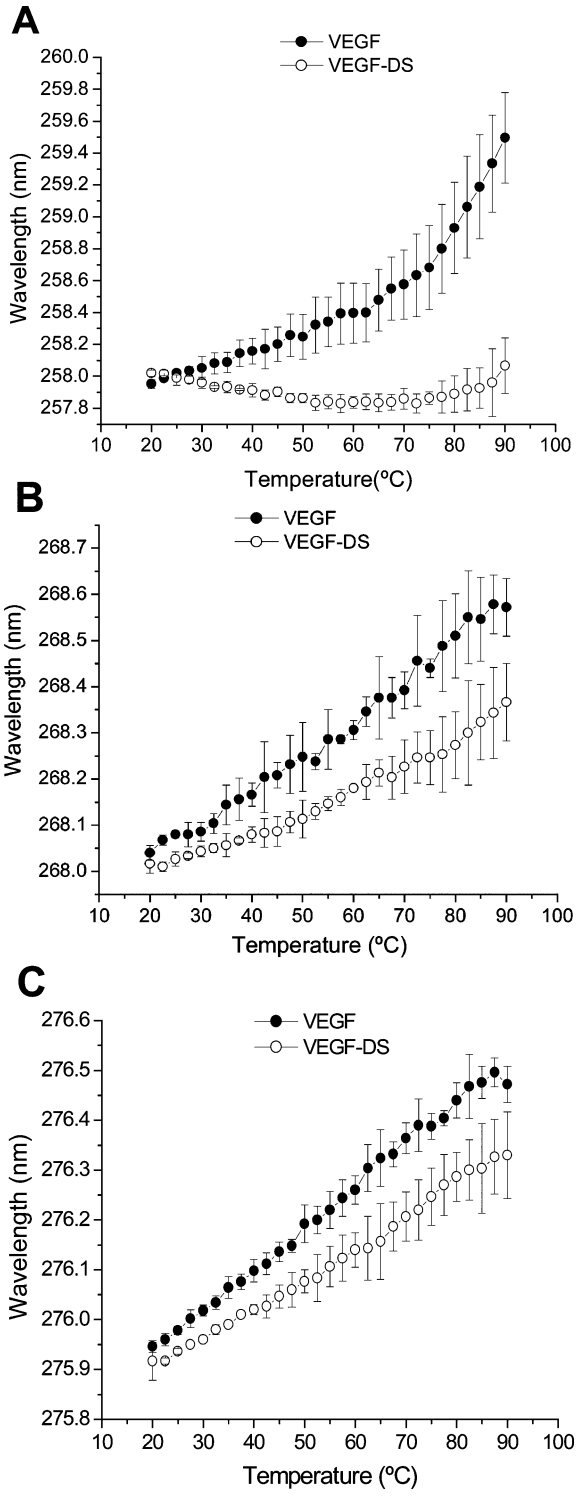

Figure 4. UV absorbance revealed the effect of temperature on the second derivative peak (A) at 258 nm (Phe), (B) at 268 nm (Phe/Tyr), and (C) at 275 nm (Tyr) for VEGF and VEGF bound with DS ($n = 3$).

Physicochemical Characterization of Polyelectrolyte Nanoparticles and VEGF. Dextran sulfate was complexed with three polycations (chitosan, polyethylenimine, and poly-L-lysine) to determine the effect of these materials on particle size, polydispersity, zeta potential, and VEGF encapsulation efficiency. Each of these polycations vary in charge density and have a history of use as gene, peptide, and small protein delivery vehicles.[43−45] Prior to the work reported here, we systematically screened polyelectrolyte molecular weights and concentrations to determine conditions for most effectively forming ~200 nm

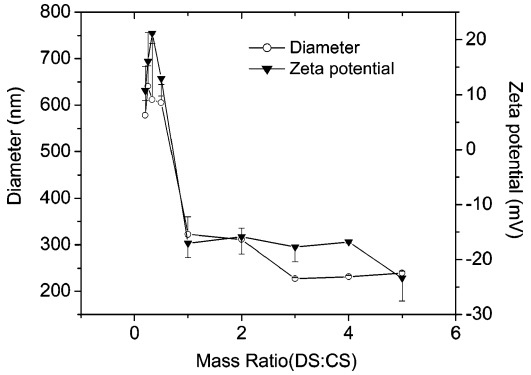

Figure 5. Varying the mass ratio of DS:CS allows control of particle size and zeta potential.

Table 1. Properties of Polyelectrolyte Nanoparticles

nanoparticle formulation	diameter (nm)	polydispersity	zeta potential (mV)	entrapment efficiency (%)
CS−DS	239 ± 4	0.18 ± 0.02	−18.4 ± 0.3	
VEGF CS−DS	284 ± 4	0.22 ± 0.05	−14.4 ± 0.5	83.3 ± 5.0
PEI−DS	209 ± 3	0.10 ± 0.01	−16.0 ± 1.9	
VEGF PEI−DS	258 ± 14	0.02 ± 0.01	−12.9 ± 0.9	48.1 ± 3.4
PLL−DS	173 ± 3	0.14 ± 0.02	−18.7 ± 2.3	
VEGF PLL−DS	159 ± 3	0.18 ± 0.01	−14.6 ± 1.5	52.2 ± 0.7

particles. Varying the mass ratio of polycation to dextran sulfate resulted in direct control over polymer complex diameter and zeta potential including the production of small (∼200 nm) complexes. Exemplary data for chitosan paired with dextran sulfate are shown (Figure 5). These trends corroborate reports in literature.[37] The results for polyethylenimine or poly-L-lysine complexed with dextran sulfate were also similar to literature reports and were examined for obtaining particles ∼200 nm in size while maintaining the same ratio of DS to polycation.[30−32] A Brookhaven ZetaPALS Zeta Potential Analyzer was used to analyze the particle size and size distribution of ∼5 mg/mL solutions of the complexes in deionized (DI) water (Table 1). Poly-L-lysine nanoparticles showed the smallest particle size under these particular fabrication conditions (see Materials and Methods). The polydispersity values for formulations of nanoparticles were all less than 0.23 at the polyelectrolyte concentrations employed, indicating reasonable size distributions for the nanoparticle formulations. Increasing polyelectrolyte concentration generally resulted in the formation of a precipitate. In general, the nanoparticle formulations possessed negative surface charges (Table 1). The encapsulation of VEGF does not seem to significantly change the size and zeta potential of the PEC nanoparticles studied. TEM images provide supporting evidence of the particle size and insight into the particle morphology (Figure 6).

FTIR was employed in this study to further explore the structures of VEGF, the individual polyelectrolytes, and the complexed nanoparticles. The VEGF spectrum shows the signature amide I (1700−1600 cm^{-1}) and amide II bands (1600−1500 cm^{-1}) of the protein (Figure 7A and Supporting Information Figure 1A). These bands were deconvoluted to determine the secondary structure composition of VEGF in the presence and absence of DS (Figure 7 and Table 2). This analysis demonstrated that VEGF's secondary structure consists primarily of β-sheet and β-turn (Table 2), which is in agreement with the CD analysis. No significant changes in the secondary structure of VEGF in the presence and absence of DS were observed, thus confirming minimal perturbation of secondary structure upon VEGF binding. In the spectra of VEGF-loaded and unloaded PEC nanoparticles, the polycationic polymer and

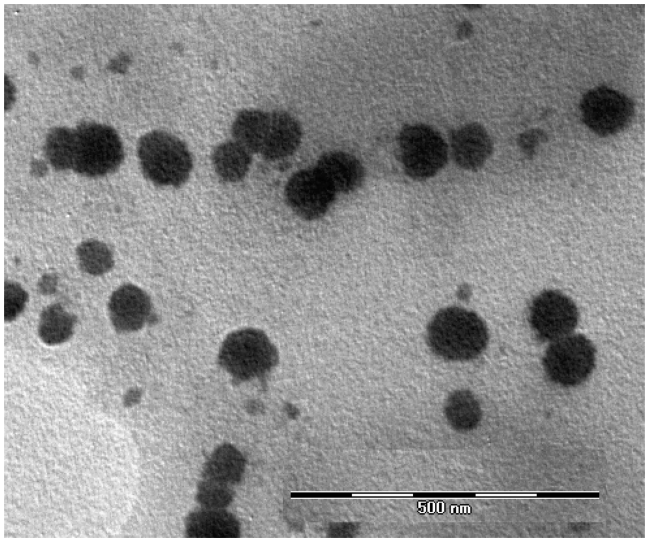

Figure 6. Transmission electron micrograph of DS:CS nanoparticles.

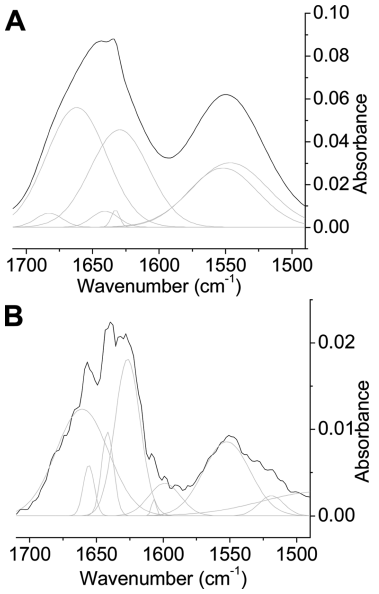

Figure 7. Deconvoluted FTIR spectra of (A) VEGF and (B) VEGF in the presence of DS. The quality of the spectrum in the presence of DS is less resolved due to the lower intensity of the amide I and II bands when DS was added. Regardless, the secondary structure of VEGF appears to retain β-sheet and β-turn structure in the presence and absence of DS.

VEGF structures are not clearly apparent (Supporting Information Figure 1C). This is likely due to the significantly greater concentration of DS (0.3% w/v) as compared to the polycation and protein concentrations (theoretically, 0.06% w/v and 0.03 mg/mL, respectively), because bands representative of S═O stretching are apparent in the PEC spectra near 1000−1050 and 1200−1300 cm^{-1}.

VEGF Entrapment, Release Kinetics, and Activity. PEC nanoparticles prepared using chitosan showed the highest entrapment efficiency of 83.3% (Table 1). The release profile of VEGF from nanoparticles demonstrated an initial burst release of ∼12% of VEGF in the first 2 h followed by a slower sustained release (Figure 8). The relatively high entrapment efficiency of chitosan−DS PECs explains why these nanoparticles show a greater amount of total VEGF release than the other two nanoparticle types. PEI−DS and PLL−DS data for the total amount of VEGF released were consistent with their entrapment efficiencies (Table 1). Approximately 75% of the

Table 2. Structural Assignment for VEGF and VEGF Bound with DS Based on FTIR Deconvolution

VEGF				VEGF−DS			
wavenumber (cm^{-1})	peak area	%	assignment	wavenumber (cm^{-1})	peak area	%	assignment
1682.5	0.17	3	β-turn	1660.5	0.61	50	β-turn
1661.8	3.15	48	β-turn	1655.6	0.06	5	α-helix
1640.5	0.19	3	β-sheet	1641.5	0.11	9	unordered
1632.6	0.06	1	β-sheet	1626.5	0.43	36	β-sheet
1629.5	2.50	38	β-sheet				

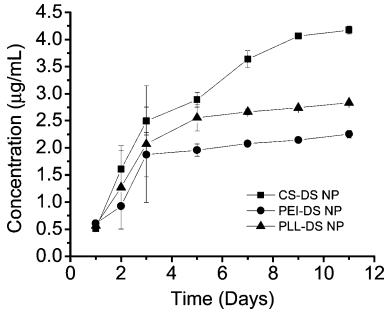

Figure 8. VEGF release profiles for CS−DS (■), PEI−DS (●), and PLL−DS (▲) showed similar trends proportional to the encapsulation efficiency of each formulation ($n = 3$).

Table 3. Percentage of "Active" VEGF Released from Nanoparticles As Determined by ELISA ($n = 3$)

nanoparticle formulation	day 1 "active" VEGF (%)	day 10 "active" VEGF (%)
VEGF CS−DS NP	97.98 ± 7.99	77.45 ± 11.88
VEGF PEI−DS NP	82.66 ± 7.31	78.94 ± 1.21
VEGF PLL−DS NP	95.54 ± 10.04	60.43 ± 11.17

encapsulated protein was released over a period of 10 days for all nanoparticle formulations. It was observed that the released protein retained its structural integrity as determined from the ELISA assay (Table 3).

VEGF bioactivity was determined in solution or as released from PEC nanoparticles using an in vitro HUVEC proliferation bioassay. The results of this assay are shown as a cell viability curve (Figure 9). HUVEC treated with VEGF in solution (100 ng/mL) showed a negligible increase in cell proliferation that was not statistically significant from controls employing no VEGF. The growth increase of cells incubated with VEGF solution is significant ($p < 0.05$) at day 2 as compared to that of the control. Conversely, cells treated with VEGF-loaded nanoparticles generally demonstrated a sustained significant increase in the cell proliferation activity with time within 5 days ($p < 0.05$ for CS, PEI, PLL nanoparticles at days 2, 3, 5). Control nanoparticles (blanks) demonstrated significantly lower proliferation activity as compared to VEGF nanoparticles, with the exception of PEI nanoparticles as mentioned above.

Cell proliferation response gradually increased with time when HUVEC was treated with VEGF-loaded nanoparticles as compared to the negligible increase observed for cells treated with VEGF in solution delivered at an equal bolus dose (100 ng/mL) at time zero. Cell proliferation was impeded by contact inhibition, which prevented further assessment of cell proliferation beyond day 4−5. This type of growth curve is common for this assay. More importantly, VEGF concentration was sustained around 3.5 ng/mL in cell media as determined from the ELISA for at least 5 days when cells were treated with VEGF-loaded nanoparticles, while the VEGF concentration in culture decreased rapidly for cells treated with VEGF in solution

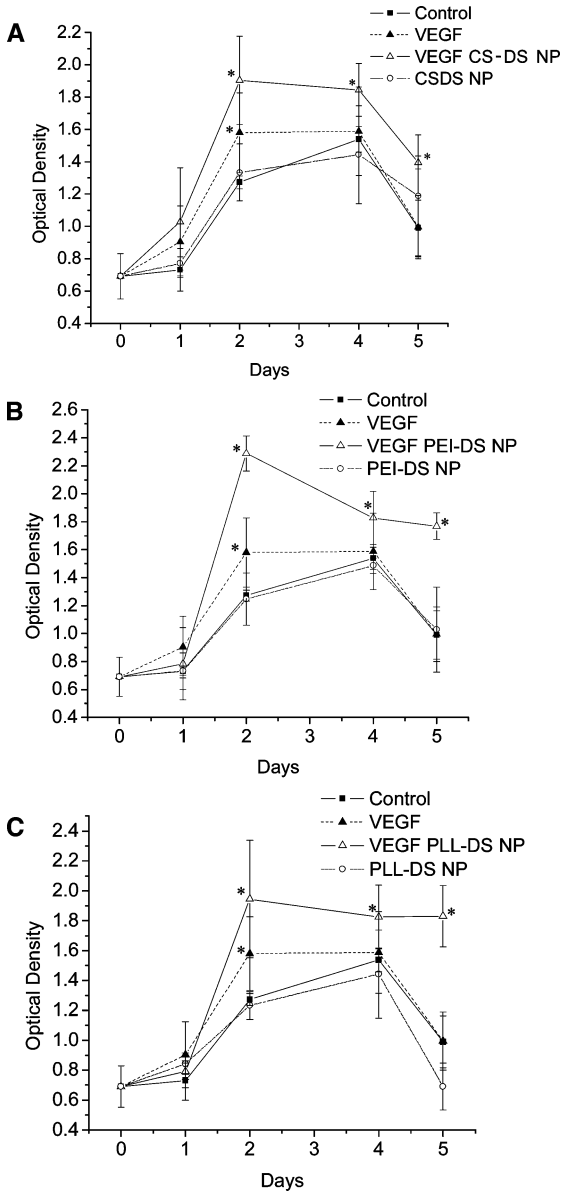

Figure 9. Sustained HUVEC proliferation effect of VEGF in nanoparticles. HUVEC was incubated with a VEGF solution or VEGF-loaded nanoparticles for 5 days. The optical density at 490 nm was recorded using MTS assay. (A) CS−DS nanoparticles, (B) PEI−DS nanoparticles, and (C) PLL−DS nanoparticles ($n = 3$).

(Figure 10). Of course, in vitro VEGF release data should not be interpreted as the total amount released from nanoparticles because much of the released VEGF will be bound to VEGF receptors or extracellular matrix (dependent upon cell density), enzymatically degraded, etc. The relatively constant concentration of VEGF may be explained by the equilibrium of free VEGF (detected), degraded VEGF, receptor-bound VEGF, and VEGF continually released from nanoparticles.

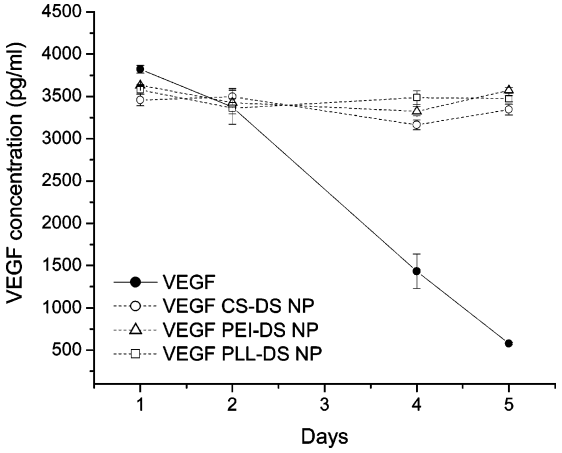

Figure 10. VEGF concentration in HUVEC medium as determined by ELISA after incubation with VEGF solution or VEGF nanoparticles ($n = 3$).

Discussion

The design of controlled release systems for the delivery of proteins poses multiple challenges. The major focus of this work is to develop a drug delivery system to effectively stabilize and controllably release VEGF using a nanocarrier administrable by IV injection. The circulation half-life of $VEGF_{165}$ is about 30 min in vivo, suggesting the necessity of controlled release administration for the induction of angiogenesis.[10] Although VEGF is inherently physically stable, maintenance of protein structure through nanoparticle processing and during release is essential. For example, proteins in general are sensitive to solvent exposure, may be especially labile at extreme pH or high temperature, degrade via hydrolysis, oxidize, etc. Of course, the bioactivity of the protein also depends on the maintenance of native structure.

In the current study, we employ an organic solvent-free method to fabricate nanoparticles that entrap stabilized VEGF. In addition, when DS with bound VEGF is electrostatically complexed with a cationic polymer such as chitosan, the resulting nanoparticles are entirely biodegradable. Dextran sulfate (DS), a biodegradable polyanion, was utilized because it has been demonstrated to bind and stabilize heparin-binding growth factors.[7,46] VEGF in solution slowly loses secondary structure during thermal melts as shown from CD data. Conversely, dextran sulfate effectively stabilizes the secondary structure of VEGF as demonstrated by the stable molar ellipticity minimum at temperatures as high as 90 °C. Maintenance of VEGF secondary structure was also observed in polyelectrolyte complexes, although these data were somewhat confounded by the inherent opacity of the nanoparticle suspension. DSC further confirmed the stabilizing effect of DS and PEC nanoparticles because these formulations did not show any thermal transition in the range of 20−115 °C. Finally, FTIR data confirmed that the structure of VEGF bound with DS is essentially unchanged as compared to the native structure of VEGF, although clear VEGF structural data were unattainable in the nanoparticle formulations.

Formulation of nanosuspensions for IV injection requires tight control over the nanoparticle size and surface charge. For example, larger nanoparticles (>500 nm) may lead to occlusions or may accumulate in filtering organs. Also, nanoparticles with a hydrophilic surface possessing a weakly negative or neutral zeta potential have been shown to minimize adsorption of opsonizing proteins, leading to a potential extension of circulation half-life.[47] Nanoparticles formulated from the three selected types of cationic polymers, CS, PEI, and PLL, demonstrated reasonable size distributions with an average diameter between ~150 and 300 nm for both blank and VEGF-loaded nanoparticles. All blank nanoparticles presented a negative surface charge with zeta potential values between −16 and −19 mV. The entrapment of VEGF into nanoparticles slightly decreased the zeta potential to around −12 to −15 mV, which is reasonable as VEGF carries a positive charge under the fabrication conditions (the isoelectric point of VEGF is 8.5).[48] This result may also suggest that some of the VEGF is located on or near the nanoparticle surface.

Differences in the entrapment efficiency were noted for the different polyelectrolytes used to condense DS with bound VEGF. Chitosan is insoluble at pH 7.4. This property may lead to increased nanoparticle rigidity, thus improving encapsulation efficiency, extending release, and reducing rapid initial release of VEGF. Alternatively, the polycations PEI and PLL possess a higher charge density in comparison to chitosan and may displace the binding of VEGF to DS. We hypothesize that similar arguments may apply to the mechanism of controlled release of VEGF. For example, polyelectrolytes are electrostatically bound to one another; however, these binding events may be interrupted by buffer salts (charge shielding) or kinetic binding−unbinding events within the nanoparticle. Similar hypotheses have been tested for polyelectrolyte multilayers, which form a "fuzzy" matrix due to interdiffusing of layers.[49] Such events may lead to nanoparticle restructuring, thus increasing the rate of VEGF beyond what would be expected for VEGF diffusion through a polyanion network.[50]

Once stable nanosuspensions containing particles possessing the correct size and surface charge have been formed, the next step is to localize the accumulation of these nanoparticles in vivo. Future work will focus on methods to develop nanoparticle targeting, but here we confirm the controlled release of active VEGF. The release of VEGF was generally slow, with more than 75% of VEGF released over 10 days. ELISA studies confirmed that around 60−80% of VEGF remains bioactive at 10 days in the release experiment, indicating that the protein encapsulated in nanoparticles was protected. A sustained effect of VEGF following its encapsulation in nanoparticles is also evident from the results of cell proliferation studies. The sustained effect of VEGF-loaded nanoparticles may be attributed to DS binding and the slow release of VEGF. VEGF concentration determined in the cell media remains around 3.5 nM for cells treated with VEGF-loaded nanoparticles as compared to the rapidly decreasing VEGF concentration for cells treated with VEGF solutions. Although the protein released from nanoparticles would also suffer from degradation, continuous release from nanoparticles may ensure the maintenance of VEGF levels in the cell culture medium. This particular dosing reflects a reported physiologically active concentration of VEGF (2−6 ng/mL).[51] VEGF formulated in this PEC nanoparticle system represents a promising method to achieve stabilized and controlled release of this potent mitogen.

Conclusions

VEGF-loaded nanoparticles were successfully formulated using self-assembled polyelectrolyte complexes based on coacervation of oppositely charged polyelectrolytes. Dextran sulfate effectively stabilizes VEGF, as evidenced from various biophysical techniques. The resulting nanoparticles efficiently encapsulate and release bioactive protein in a sustained manner. Moreover, VEGF-loaded PEC nanoparticles significantly stimu-

lated endothelial cell proliferation in comparison to VEGF in solution delivered in equal concentration. The improved efficacy of nanoencapsulated VEGF to induce cell proliferation was attributed to the fact that nanoparticles maintained a higher concentration of the active VEGF in the culture medium, a fact that was validated by ELISA confirmation of VEGF concentration in culture. This study provides insight into a nanoparticle approach for stabilizing and delivering VEGF in an effort to generate a minimally invasive, intravenous injection toward future efforts of targeted angiogenesis.

Acknowledgment. This work was partially supported through a Scientist Development Grant from the American Heart Association and through an Innovation Award from the Juvenile Diabetes Research Foundation. We would like to thank Ann Daugherty of Genentech, Inc., for graciously supplying VEGF and for a critical review of the manuscript. We also extend our thanks to Russ Middaugh for helpful discussions and for use of equipment. The Microscopy Lab has our gratitude for assisting with TEM imaging.

Supporting Information Available. FTIR structural characterization of VEGF, VEGF in the presence of DS and DS alone, the cationic polyelectrolytes, and VEGF-loaded and unloaded PECs of chitosan−DS and PEI−DS. This material is available free of charge via the Internet at http://pubs.acs.org.

References and Notes

(1) Ferrara, N.; Alitalo, K. *Nat. Med.* **1999**, *5*, 1359−64.
(2) Folkman, J. *C. R. Acad. Sci. III* **1993**, *316*, 909−18.
(3) Ware, J. A.; Simons, M. *Nat. Med.* **1997**, *3*, 158−64.
(4) Simons, M.; Ware, J. A. *Nat. Rev. Drug Discovery* **2003**, *2*, 863−71.
(5) Folkman, J. *Circulation* **1998**, *97*, 1108−10.
(6) Richardson, T. P.; Peters, M. C.; Ennett, A. B.; Mooney, D. J. *Nat. Biotechnol.* **2001**, *19*, 1029−34.
(7) Cleland, J. L.; Duenas, E. T.; Park, A.; Daugherty, A.; Kahn, J.; Kowalski, J.; Cuthbertson, A. *J. Controlled Release* **2001**, *72*, 13−24.
(8) Street, J.; Bao, M.; deGuzman, L.; Bunting, S.; Peale, F. V., Jr.; Ferrara, N.; Steinmetz, H.; Hoeffel, J.; Cleland, J. L.; Daugherty, A.; van Bruggen, N.; Redmond, H. P.; Carano, R. A.; Filvaroff, E. H. *Proc. Natl. Acad. Sci. U.S.A.* **2002**, *99*, 9656−61.
(9) Goolcharran, C.; Cleland, J. L.; Keck, R.; Jones, A. J.; Borchardt, R. T. *AAPS PharmSci.* **2000**, *2*, E5.
(10) Eppler, S. M.; Combs, D. L.; Henry, T. D.; Lopez, J. J.; Ellis, S. G.; Yi, J. H.; Annex, B. H.; McCluskey, E. R.; Zioncheck, T. F. *Clin. Pharmacol. Ther.* **2002**, *72*, 20−32.
(11) Qaum, T.; Xu, Q.; Joussen, A. M.; Clemens, M. W.; Qin, W.; Miyamoto, K.; Hassessian, H.; Wiegand, S. J.; Rudge, J.; Yancopoulos, G. D.; Adamis, A. P. *Invest. Ophthalmol. Visual Sci.* **2001**, *42*, 2408−13.
(12) Martin, A.; Komada, M. R.; Sane, D. C. *Med. Res. Rev.* **2003**, *23*, 117−45.
(13) Yang, R.; Ogasawara, A. K.; Zioncheck, T. F.; Ren, Z.; He, G. W.; DeGuzman, G. G.; Pelletier, N.; Shen, B. Q.; Bunting, S.; Jin, H. *Hypertension* **2002**, *39*, 815−20.
(14) Henry, T. D.; Annex, B. H.; McKendall, G. R.; Azrin, M. A.; Lopez, J. J.; Giordano, F. J.; Shah, P. K.; Willerson, J. T.; Benza, R. L.; Berman, D. S.; Gibson, C. M.; Bajamonde, A.; Rundle, A. C.; Fine, J.; McCluskey, E. R. *Circulation* **2003**, *107*, 1359−65.
(15) Murphy, W. L.; Peters, M. C.; Kohn, D. H.; Mooney, D. J. *Biomaterials* **2000**, *21*, 2521−7.
(16) Zisch, A. H.; Lutolf, M. P.; Hubbell, J. A. *Cardiovasc. Pathol.* **2003**, *12*, 295−310.
(17) Peirce, S. M.; Price, R. J.; Skalak, T. C. *Am. J. Physiol. Heart Circ. Physiol.* **2004**, *286*, H918−25.
(18) Rade, J. J.; Cheung, M.; Miyamoto, S.; Dichek, D. A. *Gene Ther.* **1999**, *6*, 385−392.
(19) Rosengart, T. K.; Lee, L. Y.; Patel, S. R.; Kligfield, P. D.; Okin, P. M.; Hackett, N. R.; Isom, O. W.; Crystal, R. G. *Ann. Surg.* **1999**, *230*, 466−470.
(20) Stella, B.; Arpicco, S.; Peracchia, M. T.; Desmaele, D.; Hoebeke, J.; Renoir, M.; D'Angelo, J.; Cattel, L.; Couvreur, P. *J. Pharm. Sci.* **2000**, *89*, 1452−64.
(21) Schiffelers, R. M.; Ansari, A.; Xu, J.; Zhou, Q.; Tang, Q.; Storm, G.; Molema, G.; Lu, P. Y.; Scaria, P. V.; Woodle, M. C. *Nucleic Acids Res.* **2004**, *32*, e149.
(22) Moghimi, S. M.; Hunter, A. C.; Murray, J. C. *Pharmacol. Rev.* **2001**, *53*, 283−318.
(23) Li, L.; Wartchow, C. A.; Danthi, S. N.; Shen, Z.; Dechene, N.; Pease, J.; Choi, H. S.; Doede, T.; Chu, P.; Ning, S.; Lee, D. Y.; Bednarski, M. D.; Knox, S. J. *Int. J. Radiat. Oncol. Biol. Phys.* **2004**, *58*, 1215−27.
(24) Ruoslahti, E. *Cancer Cell* **2002**, *2*, 97−8.
(25) Alavi, A.; Hood, J. D.; Frausto, R.; Stupack, D. G.; Cheresh, D. A. *Science* **2003**, *301*, 94−6.
(26) Xu, Y. Y.; Li, Y. J.; Guan, H.; Liu, C. W.; Zheng, Y. H.; Liu, B.; Yang, J.; Song, C. X. *Zhonghua Wai Ke Za Zhi* **2004**, *42*, 58−61.
(27) Bala, I.; Hariharan, S.; Kumar, M. N. *Crit. Rev. Ther. Drug Carrier Syst.* **2004**, *21*, 387−422.
(28) Sheridan, M. H.; Shea, L. D.; Peters, M. C.; Mooney, D. J. *J. Controlled Release* **2000**, *64*, 91−102.
(29) Tibbetts, S. A.; Chirathaworn, C.; Nakashima, M.; Jois, D. S.; Siahaan, T. J.; Chan, M. A.; Benedict, S. H. *Transplantation* **1999**, *68*, 685−692.
(30) Tiyaboonchai, W.; Woiszwillo, J.; Middaugh, C. R. *J. Pharm. Sci.* **2001**, *90*, 902−14.
(31) Tiyaboonchai, W.; Woiszwillo, J.; Middaugh, C. R. *Eur. J. Pharm. Sci.* **2003**, *19*, 191−202.
(32) Tiyaboonchai, W.; Woiszwillo, J.; Sims, R. C.; Middaugh, C. R. *Int. J. Pharm.* **2003**, *255*, 139−51.
(33) Miralem, T.; Steinberg, R.; Price, D.; Avraham, H. *Oncogene* **2001**, *20*, 5511−24.
(34) Folkman, J. *Proc. Natl. Acad. Sci. U.S.A.* **1998**, *95*, 9064−9066.
(35) Chupa, J. M.; Foster, A. M.; Sumner, S. R.; Madihally, S. V.; Matthew, H. W. *Biomaterials* **2000**, *21*, 2315−22.
(36) Serizawa, T.; Yamaguchi, M.; Akashi, M. *Biomacromolecules* **2002**, *3*, 724−31.
(37) Schatz, C.; Domard, A.; Viton, C.; Pichot, C.; Delair, T. *Biomacromolecules* **2004**, *5*, 1882−92.
(38) Koppel, D. E. *J. Chem. Phys.* **1972**, *57*, 4814−4820.
(39) Muller, Y. A.; Heiring, C.; Misselwitz, R.; Welfle, K.; Welfle, H. *J. Biol. Chem.* **2002**, *27*, 43410−6.
(40) Muller, Y. A.; Christinger, H. W.; Keyt, B. A.; de Vos, A. M. *Structure* **1997**, *5*, 1325−38.
(41) Compton, L. A.; Johnson, W. C., Jr. *Anal. Biochem.* **1986**, *155*, 155−67.
(42) Whitmore, L.; Wallace, B. A. *Nucleic Acids Res.* **2004**, *32* (Web Server issue), W668−73.
(43) Bozkir, A.; Saka, O. M. *J. Drug Targeting* **2004**, *12*, 281−8.
(44) Parker, A. L.; Oupicky, D.; Dash, P. R.; Seymour, L. W. *Anal. Biochem.* **2002**, *302*, 75−80.
(45) Forrest, M. L.; Koerber, J. T.; Pack, D. W. *Bioconjugate Chem* **2003**, *14*, 934−40.
(46) Fan, H.; Li, H.; Zhang, M.; Middaugh, C. R. *J. Pharm. Sci.* **2006**.
(47) Vonarbourg, A.; Passirani, C.; Saulnier, P.; Benoit, J. P. *Biomaterials* **2006**, *27*, 4356−73.
(48) Ferrara, N.; Houck, K.; Jakeman, L.; Leung, D. W. *Endocr. Rev.* **1992**, *13*, 18−32.
(49) Fredin, N. J.; Zhang, J.; Lynn, D. M. *Langmuir* **2005**, *21*, 5803−11.
(50) Pike, D. B.; Cai, S.; Pomraning, K. R.; Firpo, M. A.; Fisher, R. J.; Shu, X. Z.; Prestwich, G. D.; Peattie, R. A. *Biomaterials* **2006**, *27*, 5242−51.
(51) Nissen, N. N.; Polverini, P. J.; Koch, A. E.; Volin, M. V.; Gamelli, R. L.; DiPietro, L. A. *Am. J. Pathol.* **1998**, *152*, 1445−52.

BM061211K